

Copyright
by
Andrew Scott Thornburg
2014

The Report committee for Andrew Scott Thornburg certifies that
this is the approved version of the following report:

Capacity and Coverage of mmWave Ad Hoc Networks

APPROVED BY

SUPERVISING COMMITTEE:

Robert W. Heath, Jr., Supervisor

François Baccelli

Capacity and Coverage of mmWave Ad Hoc Networks

by

Andrew Scott Thornburg, B.S.E.

REPORT

Presented to the Faculty of the Graduate School of
The University of Texas at Austin
in Partial Fulfillment
of the Requirements
for the Degree of

MASTER OF SCIENCE IN ENGINEERING

THE UNIVERSITY OF TEXAS AT AUSTIN

August 2014

Dedicated to my grandfather, Dr. Kenneth L. Garver

Capacity and Coverage of mmWave Ad Hoc Networks

Andrew Scott Thornburg, M.S.E.
The University of Texas at Austin, 2014

Supervisor: Robert W. Heath, Jr.

Ad hoc networks provide a flexible, infrastructure-free means to communicate between soldiers in war zones, aid workers in disaster areas, or consumers in device-to-device (D2D) applications. Ad hoc networks, however, are still plagued by interference. Communication with millimeter-wave (mmWave) devices offers hope to ad hoc networks through higher bandwidth, reduced interference due to directional antennas, and a lighter interference field due to blockage. This report uses a stochastic geometry approach to characterize the one-way and two-way coverage probability of a mmWave ad hoc network with directional antennas and random blockages. The coverage probability in the presence of noise and both line-of-sight and non-line-of-sight interference is analyzed and used to derive the transmission capacity. Several reasonable simplifications are used to derive the transmission capacity. Performance of mmWave is then analyzed in terms of area spectral efficiency and rate coverage. The results show that mmWave networks support larger densities, higher area spectral efficiencies, and better rate coverage compared to microwave ad hoc networks.

Table of Contents

Abstract	v
List of Tables	viii
List of Figures	ix
Chapter 1. Introduction	1
Chapter 2. System Model	4
Chapter 3. One-Way Ad Hoc Communication	8
3.1 One-Way Coverage Analysis	8
3.1.1 LOS Interference Limited Networks	10
3.2 One-Way Capacity Analysis	11
Chapter 4. Two-way Ad Hoc Communication	13
4.1 Two-way Coverage Analysis	14
4.2 Two-Way Capacity Analysis	15
Chapter 5. Coverage and Capacity Results	17
5.1 One-Way Communication Results	18
5.1.1 General Coverage Analysis	18
5.1.2 LOS Only	22
5.1.3 Transmission Capacity	23
5.1.4 Area Spectral Efficiency	26
5.1.5 Rate Analysis	26
5.2 Two-Way Communication Results	29
5.2.1 Impact of Asymmetric Traffic	29
Chapter 6. Conclusion	33

Bibliography	34
Vita	38

List of Tables

5.1	Parameters of results.	17
-----	--------------------------------	----

List of Figures

2.1	A dipole ad hoc network with direction antennas and blockages. The typical receiver is encountering interference from other nearby transmitters. The link distances are fixed and may be blocked by a building.	5
5.1	Coverage probability of an ad hoc network with $\lambda = 5 \times 10^{-5}$	20
5.2	Coverage probability of an ad hoc network with $\lambda = 5 \times 10^{-4}$	21
5.3	Noise and NLOS interference are negligible.	22
5.4	The largest λ for a 10% outage at various SINR thresholds and dipole distances.	24
5.5	Area spectral efficiency of network with 10% outage.	25
5.6	Optimal network density for various dipole lengths, subject to 10% outage.	27
5.7	mmWave ad hoc networks provide significant increase in rate coverage over microwave networks.	28
5.8	The transmission capacity of a two-way network can be improved by allocating bandwidth in an optimal way.	30
5.9	Significant gains can be achieved by intelligently allocating bandwidth.	32

Chapter 1

Introduction

Ad hoc networks, illustrated in Fig. 2.1, consistently underperform compared to wired networks and cellular networks. A main reason is due to the self-interference created in the network. Simple protocols either create residual interference that leads to poor signal-to-interference-plus-noise ratios (SINRs) or try to coordinate transmissions leading to fewer transmission opportunities [19]. Previous work for microwave ad hoc networks has considered directional antennas or MIMO techniques to limit interference [12, 13, 17]. While these methods do improve the probability of coverage, the achievable rate is limited by the small bandwidth and interference of microwave systems. Next-generation ad hoc networks, such as high-fidelity emergency response video or device-to-device (D2D) entertainment applications, will require a reliably high data rate. Millimeter-wave systems have orders-of-magnitude more bandwidth and less interference due to signal blockage which will allow achievable rates measured in the gigabits per second [16].

In this report, we show that mmWave ad hoc networks provide good coverage and rate probability distributions for several different network densities. We consider a narrowband mmWave channel model with independent

fading and distance-dependent path-loss. Each distance is distributed according to a Poisson point process and either line-of-sight (LOS) or non-line-of-sight (NLOS) [7, 8]. The general mathematical approach is to approximate the mmWave fading power via a Gamma random variable which can be used to compute the Laplace functional of the interference field. We compare coverage distributions from derived analytical expressions with simulated results. To facilitate analysis, we propose ignoring NLOS interference and noise; we also use a second-order approximation to compute, in closed form, the optimal outage-constrained network density, or transmission capacity. The transmission capacity is the maximum spatial density of transmitters given an outage constraint [19]. The rate coverage of mmWave ad hoc networks is compared to microwave ad hoc network which shows that mmWave networks can support a much higher data rate. Additionally, as many wireless communication links require receiver to transmitter communication in the form of control messages, the *two-way* transmission is analyzed. The results indicate that optimal allocation in asymmetric situations can increase performance 50-100% with respect to equal bandwidth allocation or rate based allocation

The transmission capacity of microwave wireless systems is well studied [17–19]. The transmission capacity of microwave ad hoc networks with directional antennas was studied in [13] but relied on Rayleigh fading, which is not significant in mmWave communication [15], and did not include blockage. In [17] the transmission capacity of MIMO ad hoc networks was derived, where it was shown that the receive antennas should be used for interference can-

cellation not for spatial multiplexing. Compared to results on MIMO, power-efficient hardware architectures limit mmWave devices to simple beamforming [2]. There has been considerable work in mmWave cellular networks [1, 4, 6, 7]. Cellular networks have a specific exclusion region to prevent intra-cell interference that is not present in ad hoc networks. Previous work on mmWave ad hoc networks was largely restricted to indoor scenarios with limited range; the new 802.11ad standard is based on mmWave technology for low mobility, indoor environments without blockage [20].

Chapter 2

System Model

Consider an ad hoc network where users act as transmitter or receiver. Each user in the network has a corresponding receiver at distance r . The transmitters operate at constant power with no power control. The users within the network are points from a homogeneous Poisson point process (PPP) on the Euclidean plane, \mathbb{R}^2 , with intensity λ . The channel is accessed using an Aloha-type protocol with parameter p ; during each block, a user transmits with probability p or remains silent with probability $(1 - p)$. We define the effective density, used throughout the rest of the report, as

$$\lambda := p\tilde{\lambda}, \tag{2.1}$$

which is justified through the thinning theorem [3]. We leave the optimization of p to future work, but provide a framework to find the solution in §4.

Assumption 2.1: Directional beamforming is deployed at each node. We approximate the actual beam pattern as a sectored model, as used in [13]. The beam pattern, $G_{\theta,M,m}$, is parameterized by three values: main lobe beamwidth (θ), main lobe gain (M), and back lobe gain (m). Each interfering node is equipped with a directional antenna. Because the underlying PPP is isotropic in \mathbb{R}^2 , we model the beam-direction of the typical node and each

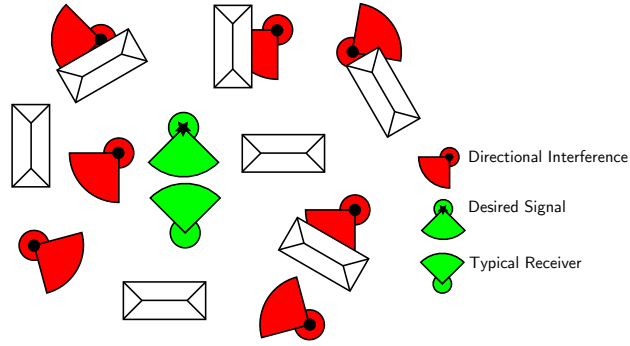


Figure 2.1: A dipole ad hoc network with direction antennas and blockages. The typical receiver is encountering interference from other nearby transmitters. The link distances are fixed and may be blocked by a building.

interfering node as a uniform random variable on $[0, 2\pi]$. Thus, the effective antenna gain of the interference seen by the typical node is a discrete random variable described by

$$M_i = \begin{cases} MM & \text{w.p. } \left(\frac{\theta}{\pi}\right)^2 \\ Mm & \text{w.p. } 2\frac{\theta}{\pi}\frac{\pi-\theta}{\pi} \\ mm & \text{w.p. } \left(\frac{\pi-\theta}{\pi}\right)^2 \end{cases}. \quad (2.2)$$

Furthermore, we assume that the typical dipole performs perfect beam alignment and thus has an antenna gain of MM .

Assumption 2.2: The signal path can be either unobstructed/LOS or blocked/NLOS, each with a different path-loss exponent. This distinction is supported by empirical measurements conducted in Austin and Manhattan [14, 15]. It was shown that by using a random shape model of buildings to model blockage [9], the probability that a communication link is LOS is $\mathbb{P}[\text{LOS}] = e^{-\beta d}$, where β is a parameter of density of buildings, and d is the link length. We ignore correlations between blockages, as in [8]; each blockage is determined

independently. It was shown that the difference in the performance analysis is small when ignoring the correlation [9]. The path-loss exponent on each interfering link is a discrete random variable described by

$$\alpha_i = \begin{cases} \alpha_L & \text{w.p. } e^{-\beta d_i} \\ \alpha_N & \text{w.p. } 1 - e^{-\beta d_i} \end{cases}, \quad (2.3)$$

where α_L and α_N are the LOS and NLOS path-loss exponents.

Assumption 2.3: We assume that the typical node link is LOS for simplicity of the analysis. This follows from the equivalent LOS ball approach of [5]. In such a network, the number of LOS nodes with respect to the origin is > 1 . Thus, it is reasonable to expect the desired link to be LOS.

Assumption 2.4: Nakagami fading is assumed for LOS links. In the measurements of [14, 15], Rayleigh fading is not strongly exhibited. The claim was made that mmWave analysis can ignore fading. To help with the analytical tractability, we model the fading as a Nakagami random variable with parameter N . Consequently, the received signal power can be modeled as a Gamma random variable. As $N \rightarrow \infty$, the fading becomes a deterministic value centered on the mean, whereas $N = 1$ corresponds to Rayleigh fading. This assumption makes the analysis quite general, and flexible.

To analyze such a network, we must precisely define the coverage probability. Specifically, we are interested in $\mathbb{P}[\text{SINR} > T]$ where T is the threshold for successful packet transmission. The SINR is defined as

$$\text{SINR} = \frac{P_t M_0 h_0 r^{-\alpha_0}}{N_0 + \sum_{i \in \Phi} P_t M_i h_i d_i^{-\alpha_i}} \quad (2.4)$$

where P_t is the transmit power of each dipole, M_0 is the antenna gain corresponding to both main beams aligned, h_0 is the fading at the dipole of interest, r is the fixed dipole link length, α is the path-loss exponent, and N_0 is the noise power. The terms within the sum are for each interfering dipole transmitter; d_i is used to represent the distance from the interferer to transmitter of interest, h_i is the fading field, and M_i is the discrete random antenna gain.

Additionally, it is useful to discuss λ as the average *neighbor* distance which allows some intuition to the spacing of nodes. In \mathbb{R}^2 , this is defined as $d_n = 1/\sqrt{\pi\lambda}$. Additionally, we define the expected number of LOS interfering nodes as $\rho = \mathbb{E}[\#\text{LOS}] = 2\pi\lambda/\beta^2$, which follows as a direct result of Campbell's Theorem [7].

Chapter 3

One-Way Ad Hoc Communication

In this chapter, we will derive the coverage probability for the one-way transmission in the ad hoc network described in chapter 2. The coverage probability is analyzed using an approximation for the CDF of a gamma random variable. Next, using a 2^{nd} order Taylor expansion, the transmission capacity is derived. Using this the area spectral efficiency is obtained. In chapter 5, numerical plots of results are presented.

3.1 One-Way Coverage Analysis

Using tools from stochastic geometry, we derive the SINR distribution of the typical node of a mmWave ad hoc network located at the origin. The node has coverage if its received SINR is greater than a threshold. More formally, the coverage is

$$P_c = \mathbb{P}[\text{SINR} > T]. \quad (3.1)$$

Using (2.4),

$$P_c = \mathbb{P}\left[\frac{P_t M_0 h_0 r^{-\alpha_0}}{N + \sum_{i \in \Phi} P_t M_i h_i d_i^{-\alpha_i}} > T\right] \quad (3.2)$$

$$= \mathbb{P}\left[h_0 > \frac{T r^{\alpha_0}}{P_t M_0} \left(N + \sum_{i \in \Phi} \frac{P_t M_i h_i}{d_i^{\alpha_i}}\right)\right] \quad (3.3)$$

$$= \mathbb{P}\left[h_0 > \frac{T r^{\alpha_0}}{P_t M_0} (N + I_\Phi)\right] \quad (3.4)$$

where the interference field, I_Φ , is $I_{\Phi_{\text{LOS}}} + I_{\Phi_{\text{NLOS}}}$ by the Thinning Theorem, and are thus independent. Following the approach of [5, 7],

$$P_c \approx \sum_{n=1}^N (-1)^{n+1} \binom{N}{n} e^{-nKT N_0} \mathbb{E}_{I_{\Phi_L}} [e^{-nKT I_{\Phi_L}}] \times \mathbb{E}_{I_{\Phi_N}} [e^{-nKT I_{\Phi_N}}] \quad (3.5)$$

where $K = \frac{\eta r^{\alpha_0}}{M_0}$, and $\mathbb{E}_{I_{\Phi_L}}, \mathbb{E}_{I_{\Phi_N}}$ are the Laplace functionals of the LOS and NLOS interference fields, respectively. The LOS field can be computed as

$$\mathbb{E}_{I_{\Phi_L}} = \exp\left(-2\pi\lambda \sum_{k=1}^4 b_k \times \int_0^\infty (1 - 1/(1 + a_k nKT/x^{\alpha_L}/N)^N) e^{-\beta x} x dx\right), \quad (3.6)$$

where b_k is the thinning due to antenna gain configuration from (2.3), a_k is the corresponding normalized gain $a_k \in \{\frac{mm}{MM}, \frac{m}{M}, 1\}$, α_L is the LOS path-loss, and the interference field is computed without an exclusion zone, in contrast to the cellular approach in [5, 7]. Thus the LOS Laplace functional is

$$\mathbb{E}_{I_{\Phi_L}} = e^{-2\pi\lambda \sum_k b_k P(r, T, n)}. \quad (3.7)$$

Note that $P(r, T, n)$ is clearly a function of more than simply r and T , but link distances and the SINR threshold are the two parameters we wish to vary while analyzing the network in chapter 5. Similarly, we can compute the NLOS Laplace functional as

$$\mathbb{E}_{I_{\Phi_N}} = \exp\left(-2\pi\lambda \sum_{k=1}^4 b_k \times \int_0^\infty (1 - 1/(1 + a_k n K T / x^{\alpha_N} / N)^N) (1 - e^{-\beta x}) x dx\right), \quad (3.8)$$

where α_N is the NLOS path-loss. The Laplace Functional of the NLOS interference field is

$$\mathbb{E}_{I_{\Phi_N}} = e^{-2\pi\lambda \sum_k b_k Q(r, T, n)}. \quad (3.9)$$

Further simplifying yields the final coverage probability as

$$P_c = \sum_{n=1}^N (-1)^{n+1} \binom{N}{n} e^{-n K T N_0} e^{-2\pi\lambda \sum_k b_k (P(\cdot) + Q(\cdot))}. \quad (3.10)$$

3.1.1 LOS Interference Limited Networks

Because of the differing NLOS and LOS path loss, for network densities and building densities such that $\rho := \mathbb{E}[\#\text{LOS}] \geq 1$, the network is considered LOS Interference Limited. As such, we can neglect the noise and NLOS interference. As a result of the low LOS path loss, and correspondingly lower distance (i.e shorter links are less likely to be blocked), the LOS interference is generally several orders-of-magnitude greater than either the noise power or NLOS interference. This further simplifies the coverage probability equation

to

$$P_c = \sum_{n=1}^N (-1)^{n+1} \binom{N}{n} e^{-2\pi\lambda \sum_k b_k P(r,T)}. \quad (3.11)$$

This result is verified empirically in chapter 5. For the remainder of the analysis, we will assume a LOS Interference Limited network.

3.2 One-Way Capacity Analysis

Next, we wish to characterize the transmission capacity, λ_ϵ . This is the largest λ the network can support given an SINR threshold, T and outage ϵ . More simply, $1 - \epsilon$ of users will have an SINR larger than T . To do this, we simplify (3.10) as

$$P_c \approx \sum_{n=1}^N (-1)^{n+1} \binom{N}{n} \left(1 - 2\pi\lambda\Theta(\cdot) + 2\pi\lambda^2\Theta^2(\cdot) \right) \quad (3.12)$$

where $\Theta(\cdot) = \sum_k b_k P(r, T, n)$. We leverage the approximation, $e^x \approx (1 + x + x^2/2)$ for small x , for the Laplace functional term. We rationalize this because we are interested in analyzing the optimal λ for P_c near 1. As a result, the Laplace functional will be close to 1; the argument will be close to 0. A second order approximation is used as the first order approximation is not close for larger outage when the Laplace functional is approximately 0.5. Because of this approximation, P_c is now a quadratic equation in λ which can be solved in closed-form.

Area spectral efficiency is a useful metric because it can characterize the network performance, rather than just a single link, as SINR does. We

define area spectral efficiency as

$$\text{ASE} := \underbrace{\lambda_\epsilon}_{\frac{\text{users}}{\text{area}}} \underbrace{\log_2(1+T)}_{\text{getting rate } R} \underbrace{(1-\epsilon)}_{\% \text{ of the time}} . \quad (3.13)$$

Substituting the solution to (3.12) into (3.13) yields a function of just T and ϵ .

Chapter 4

Two-way Ad Hoc Communication

The derivations from the chapter 3 are for *one-way* communication. There is no consideration for the reverse link (i.e. receiver to transmitter). In real systems, however, successful transmission usually relies on a two-way communication link. On multiple layers of a communication link, control packets are generally used. Wireless LAN and TCP use acknowledgment packets for instance. Upon successful reception of a message, the receiver will acknowledge the success with a short *ACK* message. If the transmitter does not receive the *ACK*, it will attempt to re-send the message. A successful exchange, therefore, involves the receiver successfully decoding the large data packet *and* the transmitter successfully decoding the control message. This is two-way communication. The two-way transmission capacity quantifies the maximum density of users a network can support while *both* the forward and reverse link are subject to outage constraint, ϵ .

The same network from Fig. 2.1 is considered. The *forward* link is defined as the transmitter to receiver link (i.e. what was discussed in chapter 3), while the *reverse* link is the receiver to transmitter control link. Frequency division duplexing is used between the forward and reverse links. Consider the

bandwidth from chapter 3 split among the forward and reverse links. Hence, B_{total} is the bandwidth available to the system. The forward link is allocated B_{F} , while the reverse link is allocated $B_{\text{R}} := B_{\text{total}} - B_{\text{F}}$. The SINR is similarly defined as SINR_{F} and SINR_{R} . Correspondingly, from Shannon's equation, the links achieve rates, R_{F} and R_{R} .

4.1 Two-way Coverage Analysis

The two-way coverage probability is the probability that the forward link *and* reverse link exceed an SINR threshold. More precisely,

$$P_c^{\text{tw}} = \mathbb{P}[\text{SINR}_{\text{F}} > T_{\text{F}}, \text{SINR}_{\text{R}} > T_{\text{R}}]. \quad (4.1)$$

We assume that the forward and reverse link do not have the same SINR threshold because the reverse control link is generally low-rate compared to the forward link. In order to analyze this probability, we leverage the following definitions and lemma.

Definition 4.1 [18]: A random variable X defined on $(\Omega, \mathcal{F}, \mathbb{P})$ is increasing if $X(\omega) \leq X(\omega')$ for a partial ordering on ω, ω' . X is decreasing if $-X$ is increasing.

Let ω be a set of active interferes from the PPP. Then, $\omega' \geq \omega$ if ω' is a superset of ω . The SINR (2.4) decreases if another interferer is added: $\text{SINR}(\omega) \geq \text{SINR}(\omega')$. Thus, SINR is a decreasing random variable.

Definition 4.2[18]: An event A from \mathcal{F} is increasing if $\mathbb{I}_A(\omega) \leq \mathbb{I}_A(\omega')$ when $\omega \leq \omega'$. The event is decreasing if A^c is increasing.

The coverage probability event, $\{\text{SINR} > T\}$ is a decreasing event. Now, we can use the Fortuin, Kastelyn, Ginibre (FKG) inequality [11].

Lemma 4.1[11]: If both $A, B \in \mathcal{F}$ are increasing or decreasing events then $P(AB) \geq P(A)P(B)$.

The FKG inequality can give a lower bound on the two-way coverage probability. In [18], this was shown to be a very tight lower bound. Using FKG, we can define the two-way coverage probability as

$$P_c^{\text{tw}} \geq \mathbb{P}[\text{SINR}_F > T_F] \mathbb{P}[\text{SINR}_R > T_R]. \quad (4.2)$$

4.2 Two-Way Capacity Analysis

Using a similar approach as with the *one-way*, we use a Taylor expansion of the exponential function to yield

$$P_c^{\text{tw}} \approx \left[\sum_{n=1}^N (-1)^{n+1} \binom{N}{n} \left(1 - 2\pi\lambda\Theta(T_F) + 2\pi\lambda^2\Theta^2(T_F) \right) \right] \times \left[\sum_{n=1}^N (-1)^{n+1} \binom{N}{n} \left(1 - 2\pi\lambda\Theta(T_R) + 2\pi\lambda^2\Theta^2(T_R) \right) \right]. \quad (4.3)$$

This yields a quartic equation in λ which has an analytic expression. The general solution, however, is quite messy, and the equation would likely be

a page long, so it is omitted here. An analytical solver, such as *Mathematica*, can easily factor the coefficients of (4.3) which can be input into a polynomial root solver to yield the transmission capacity λ_ϵ . The two-way area spectral efficiency can be defined as

$$\text{ASE}_\epsilon^{\text{tw}} := \lambda_\epsilon \left(\frac{R_{\text{F}} + R_{\text{R}}}{B_{\text{total}}} \right) (1 - \epsilon). \quad (4.4)$$

The interest then becomes, given rate requirements R_{F} and R_{R} , what is the allocation of bandwidth that maximizes (4.4). We explore this trade-off in chapter 5.

Chapter 5

Coverage and Capacity Results

We first compare our analytical expression to a Monte Carlo simulation to show that it is indeed a good representation of the coverage probability. We show the results for a network with and without NLOS and noise. We then present the results for the transmission capacity, λ_c . Further, we compute the area spectral efficiency in order to define the *best* λ , λ^* . We compare the achievable rates for mmWave networks with classic results for microwave ad hoc networks. The chapter is concluded with an investigation into two-way communication. The results indicate that simply performing equal bandwidth allocation or rate-proportional allocation is sub-optimal in asymmetric two-way communication. Table 5.1 shows the values used throughout the chapter.

Parameter	Value
λ	$5 \times 10^{-5}, 5 \times 10^{-4}$
r	50, 100, 150
$\beta, \alpha_{\text{LOS}}, \alpha_{\text{NLOS}}$	0.008, 2, 4
N_0	-100 dB
h_i	Gamma w.p 3
θ, M, m	$\frac{\pi}{6}, 8, 0.125$
P_t	1W (30dBm)
N, η	3, 1.65

Table 5.1: Parameters of results.

5.1 One-Way Communication Results

For the parameters above, namely α_L and α_N , the integrals from (3.10) can be computed in closed-form. Because of the lack of exclusion zone, the integral in (3.6) can be computed in closed-form as

$$P(r, T, n) = \frac{1}{\beta^2} - \frac{a_k n K T G_{1,3}^{3,1} \left(\frac{a_k n K T \beta^2}{4N} \middle| \begin{matrix} -N \\ -1, 0, 1/2 \end{matrix} \right)}{2\sqrt{\pi}\Gamma(1+N)} \quad (5.1)$$

where $G(\cdot|\cdot)$ is the Meijer G function. Additionally, the NLOS integral is

$$Q(r, T, n) = \frac{\sqrt{N a_k n K T \pi} \Gamma(\frac{1}{2} + N)}{2\Gamma(1+N)} - \frac{1}{\beta^2} + \frac{\sqrt{a_k n K T / N} G_{1,5}^{5,1} \left(\frac{a_k n K T \beta^4}{256N} \middle| \begin{matrix} 1/2 - N \\ -1/2, 0, 1/4, 1/2, 3/4 \end{matrix} \right)}{4\sqrt{2\pi^3}\Gamma(N)} \quad (5.2)$$

These equations can be readily evaluated in software such as *MATLAB* or *Mathematica*.

5.1.1 General Coverage Analysis

First, we compare our analytical solution in (3.10) to an empirical distribution of (2.4) obtained via simulation. For the following results, Table 5.1 lists the values used to obtain the results. The parameters of (2.4) are simulated through Monte Carlo, while (3.10) is used for the analytical model. For the simulation, a PPP was generated over an area of 4km^2 , which we believe to be large enough when compared to the selected dipole lengths.

We used Gamma of order 3 for the fading in the analytical model with an $\eta = N(N!)^{(-1/N)}$ as shown in [7]. In the simulation, no fading is used.

Fig. 5.1 shows the comparison for the analytical SINR distribution with the empirical given a $\lambda = 0.00005$ or $d_n \approx 80$. In this network, $\rho \approx 5$, but the performance is still fantastic. This can be attributed to the directional antennas limiting the interference seen by the typical node. For $r = 50\text{m}$, the analytical expression yields nearly the same coverage as the simulation. The difference for $r = 100\text{m}$ is about 1 dB for small SINR, but increases to 2-3 dB for SINR above 15 dB. The analytical expression is less accurate for $r = 150\text{m}$, the difference is 5 dB for SINR greater than 10 dB; yet, for small outage probabilities, the difference between the analytical expression and simulation is 2-3 dB.

Fig. 5.2 compares the coverage distribution results for a much denser network; a $\lambda = 0.0005$ which corresponds to $d_n \approx 25$, and $\rho \approx 50$. The analytical expression provides a very good approximation for the three link lengths shown. While the coverage is seemingly much worse for this dense network, the achievable rate is still quite high. Because of the large antenna array gain of mmWave, the interference strength is not entirely devastating even with 50 users within the LOS of the typical node. The run-time of the analytical expression was much better compared to the simulation in this denser network. The data for Fig 5.2 from (3.10) was generated in 30 secs whereas the simulation was created in several minutes. This difference increases greatly with the number of nodes.

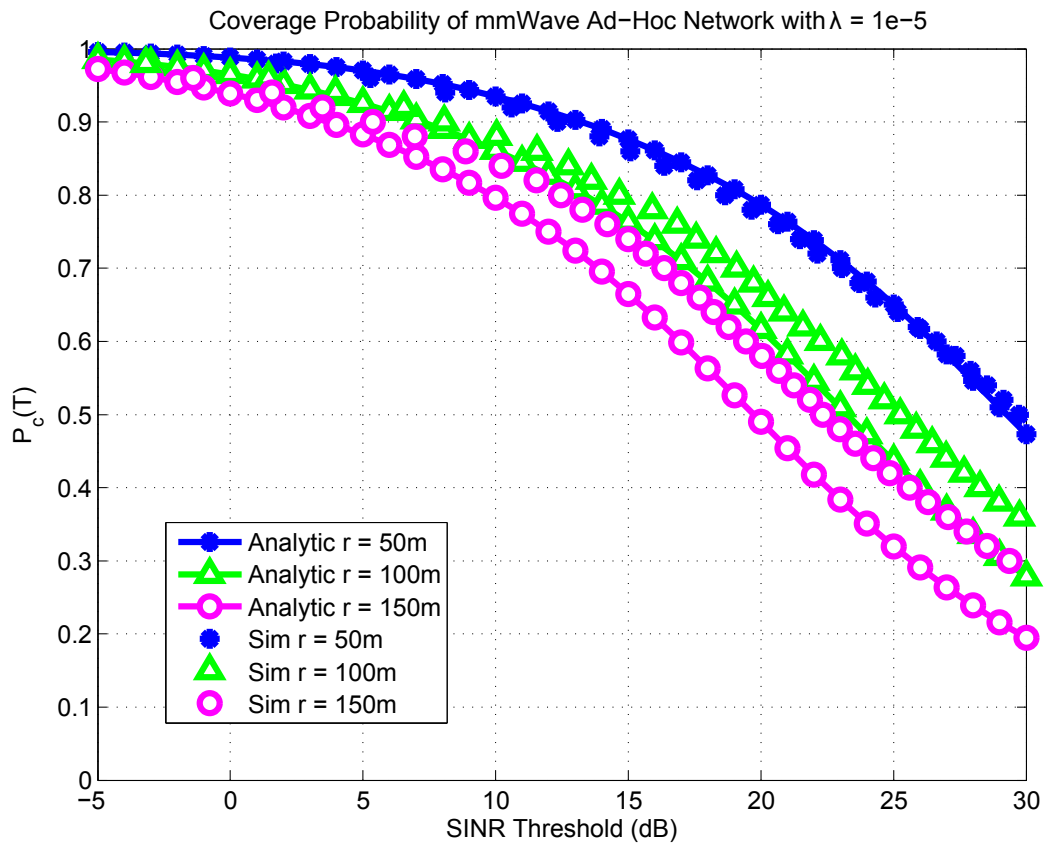


Figure 5.1: Coverage probability of an ad hoc network with $\lambda = 5 \times 10^{-5}$

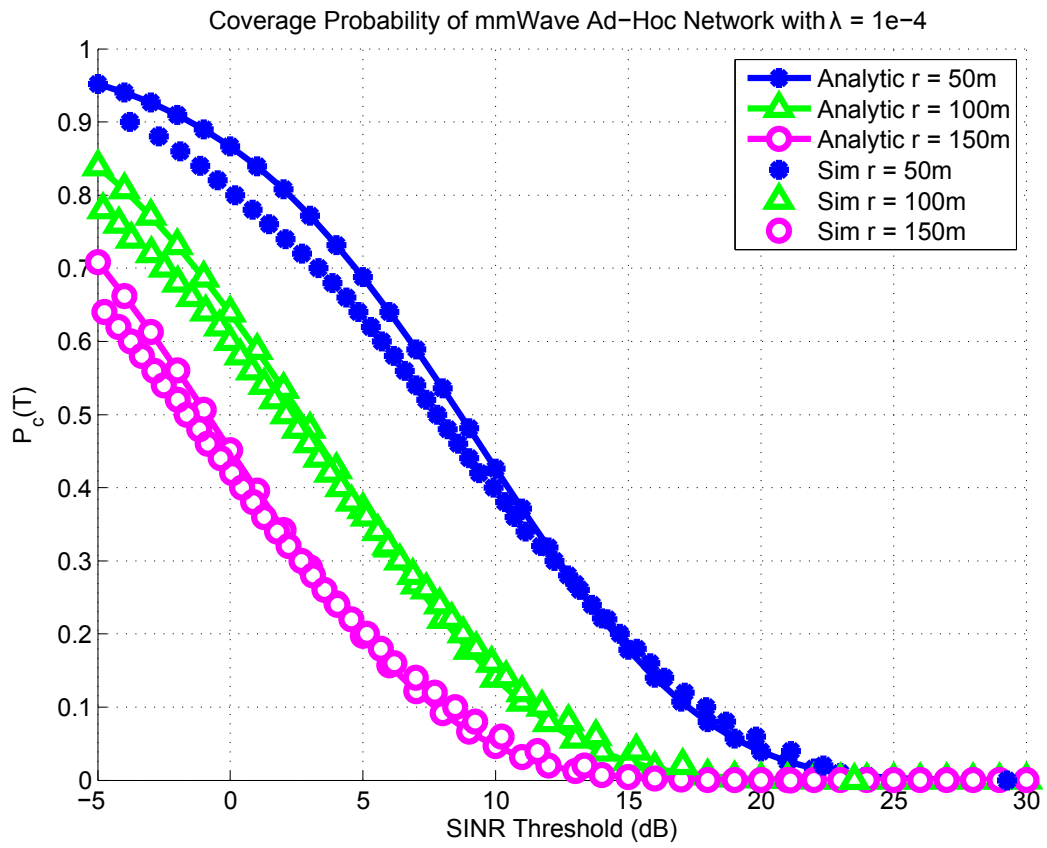


Figure 5.2: Coverage probability of an ad hoc network with $\lambda = 5 \times 10^{-4}$

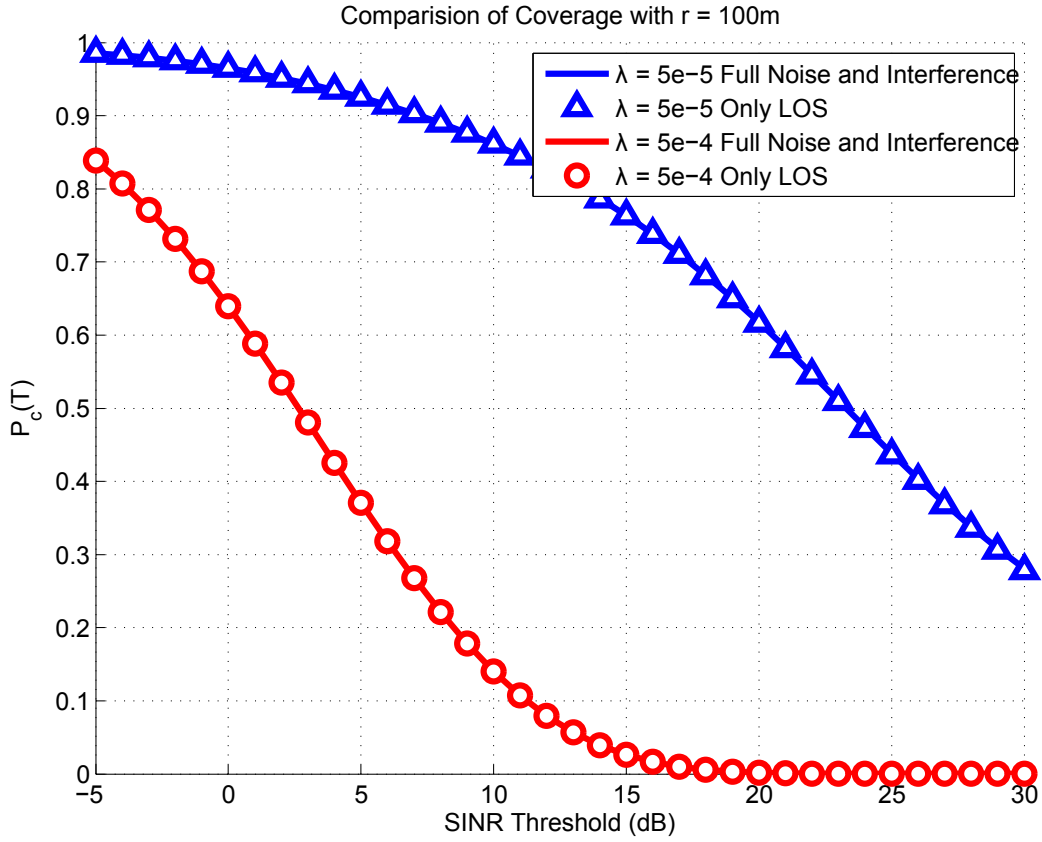


Figure 5.3: Noise and NLOS interference are negligible.

5.1.2 LOS Only

In the subsequent results, we argue that noise and NLOS interference is negligible with respect to the LOS interference strength. Using the analytical (3.10), Fig. 5.3 shows the difference using for $r = 100\text{m}$ for the values of λ . As shown, the points without noise and NLOS interference lie nearly directly on the line. While not shown, the simulation results indicate the same conclusion.

5.1.3 Transmission Capacity

Using $N = 3$, as was shown to be a tight approximation, and solving for λ yields

$$\lambda_\epsilon = \frac{-U + \sqrt{U^2 + 4\epsilon V}}{2V} \quad (5.3)$$

with $U = 6\Theta(r, T, 1)\pi - 6\Theta(r, T, 2)\pi + 2\Theta(r, T, 3)\pi$, and $V = -6\Theta^2(r, T, 1)\pi^2 + 6\Theta^2(r, T, 2)\pi^2 + 2\Theta^2(r, T, 3)\pi^2$. Some care must be taken when using (5.3) because of the existence of two solutions (which both may be < 1 and positive). In (5.3), we only take the positive solution as V is negative and the negative solution leads to a larger λ . In practice, this solution would yield a hyperdense network (e.g. average n radius $< 10m$). To solve for the density of nodes required, with an outage constraint ϵ , given the building density β , and SINR threshold T , (5.3) is used.

Fig. 5.4 shows the relationship between providing a higher SINR (and thus rate) to users while maintaining a constant outage constraint. As expected, the shortest dipole length can support the highest density of users. A linear increase in SINR (in dB) results in an exponential decrease in the density of users in the network. We include a comparison with microwave ad hoc networks [3]. The mmWave network can support a much higher density of nodes. A natural question is to ask which λ_ϵ is the best? Next, we will leverage the area spectral efficiency to answer this question.

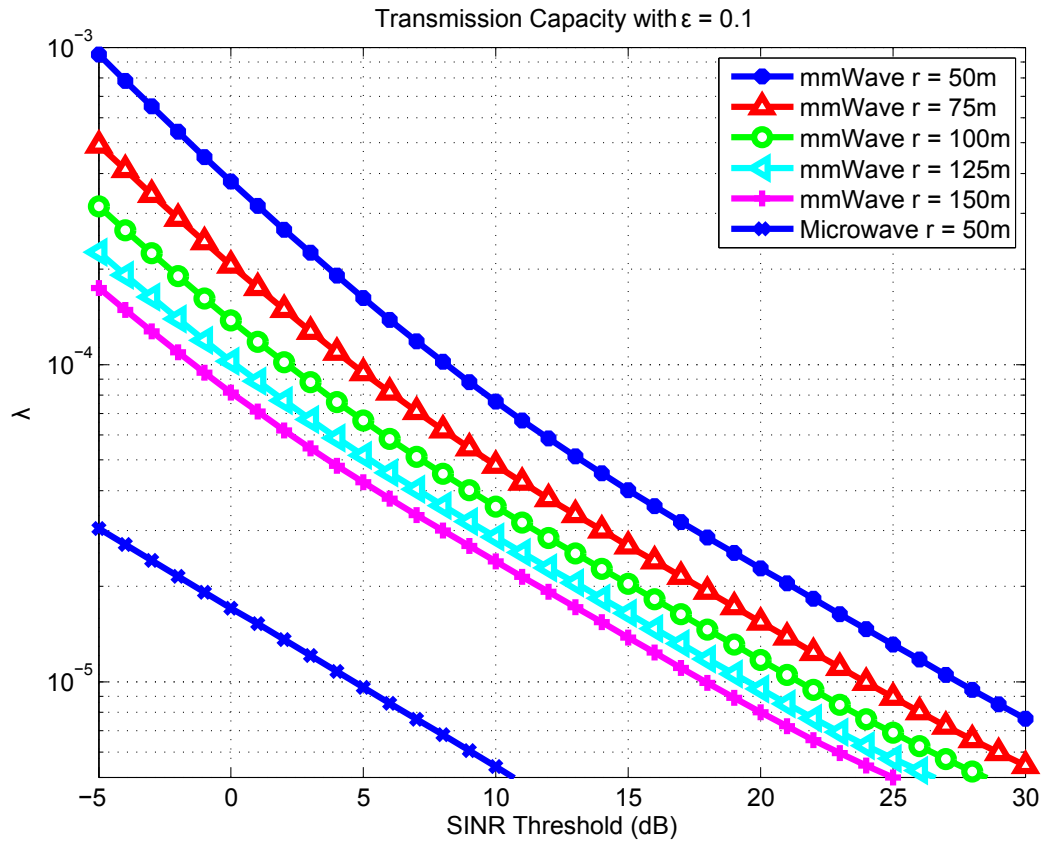


Figure 5.4: The largest λ for a 10% outage at various SINR thresholds and dipole distances.

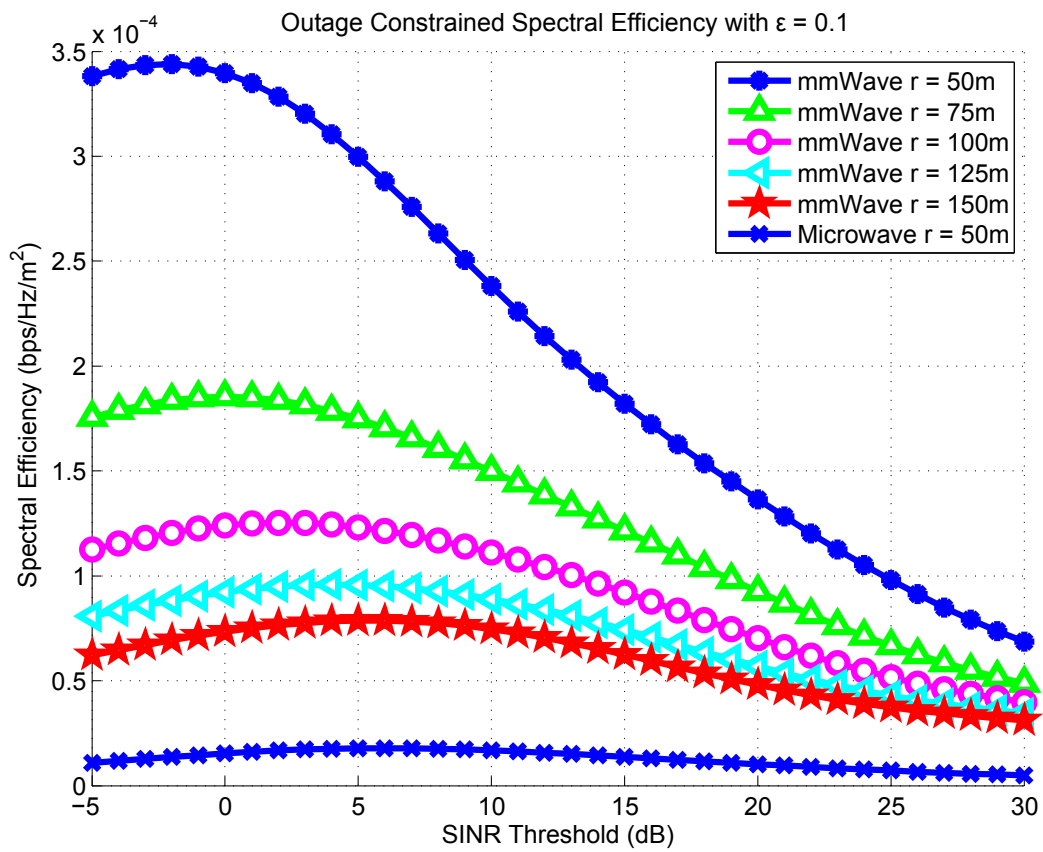


Figure 5.5: Area spectral efficiency of network with 10% outage.

5.1.4 Area Spectral Efficiency

Fig. 5.5 shows the area spectral efficiency of an ad hoc network with a 10% outage constraint. If a larger outage can be tolerated, the ASE is 50-100% higher in the 20% outage case (not shown). Additionally, increasing the link length from 50 to 75 decreases the ASE substantially. The shape of the curves suggests an optimal density with respect to ASE. This leads to the optimization problem

$$\lambda^* = \operatorname{argmax}_{\lambda_\epsilon} \lambda_\epsilon \log_2(1 + T)(1 - \epsilon) \quad (5.4)$$

We leave the exploration of solutions to this problem for future work. Fig. 5.6 shows the numerically obtained λ^* from Fig. 5.5. Notice that if the dipole length is 50, the optimal density is about what was shown in Fig. 5.2 while a dipole length of 150 optimal density is roughly what was shown in Fig. 5.1. Furthermore, the optimal density is exponentially decreasing in r .

5.1.5 Rate Analysis

Lastly, we wish to analyze the rate achieved by mmWave ad hoc networks. As alluded to earlier, the potential for extremely high data rates is real with mmWave networks. Fig. 5.7 shows the rate coverage probability, where $R = W \log_2(1 + T)$, and W is the system bandwidth.

The system bandwidth used in Fig. 5.7 is 100MHz for the mmWave and 20MHz for the microwave system. While the bandwidth is only a $5\times$ increase, we see orders of magnitude increase in the rate coverage for mmWave (note

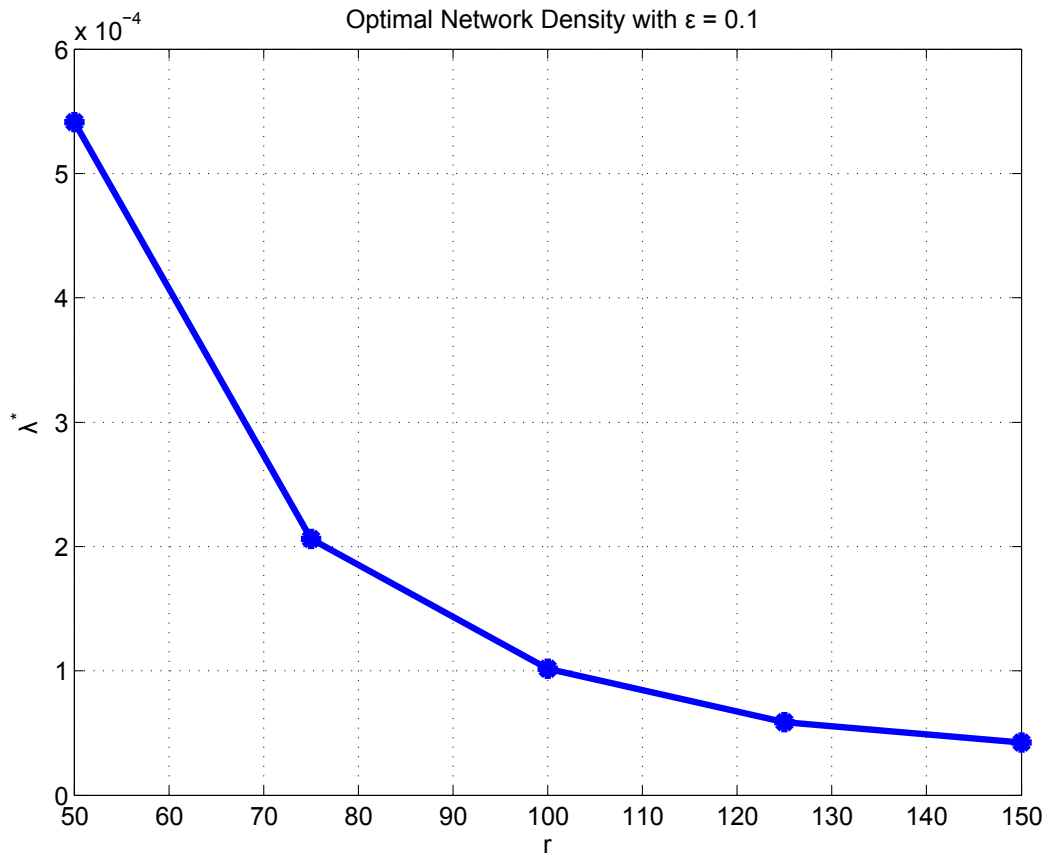


Figure 5.6: Optimal network density for various dipole lengths, subject to 10% outage.

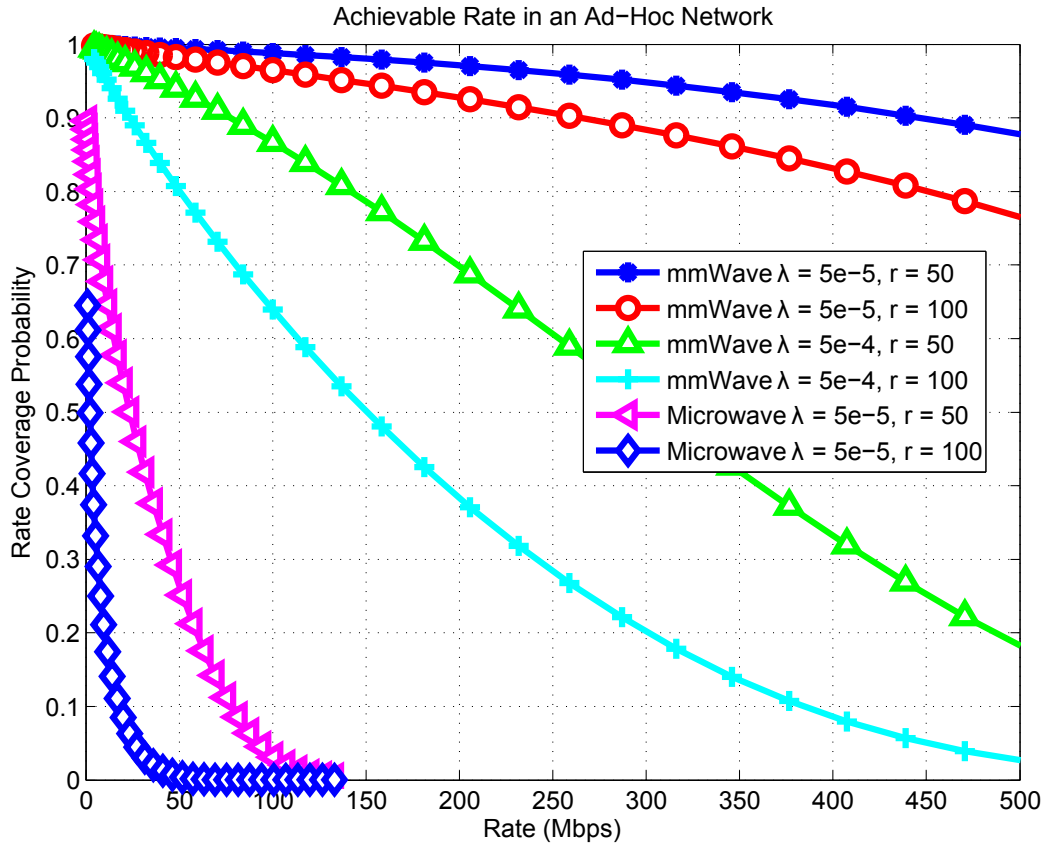


Figure 5.7: mmWave ad hoc networks provide significant increase in rate coverage over microwave networks.

the densities: the higher density microwave network barely appeared on the plot and was omitted). Because of the propagation properties of the higher frequency wave, this reduces or eliminates much of the interference.

5.2 Two-Way Communication Results

The results presented in this section consider a system under rate constraints. We show that, in asymmetric traffic, the transmission capacity of a two-way network is can be vastly improved compared to equal bandwidth allocation or rate-proportional allocation. The two-way area spectral efficiency is compared to one-way area spectral efficiency. We show that 75% of the one-way efficiency can be achieved for outage of 10% which is a 100% increase over the baseline equal allocation. In all the results, the dipole link length is 50m.

5.2.1 Impact of Asymmetric Traffic

We consider asymmetric traffic. For example, in TCP assuming 1000 byte data packets, the receiver must reply with 40 byte *ACK* packets [10]. Hence, the rate asymmetry in TCP is 1/25. The following results consider a system bandwidth of 100MHz, a forward rate requirement of 200Mbps, and a reverse link rate requirement of 8Mbps.

Fig. 5.8 shows the transmission capacity as a function of forward bandwidth allocation. As more bandwidth is added to the forward link, the required SINR_F decreases to meet the rate requirement. Because the reverse link rate

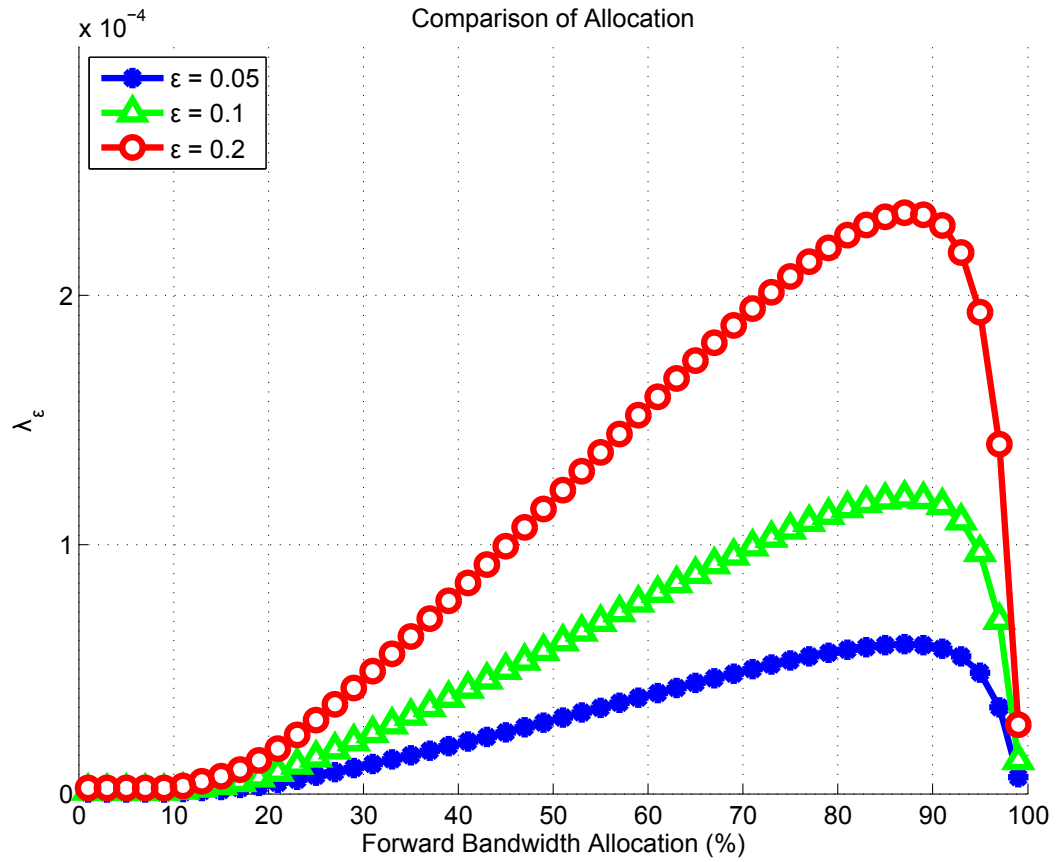


Figure 5.8: The transmission capacity of a two-way network can be improved by allocating bandwidth in an optimal way.

requirement is quite small, the increase in SINR_R does not change the coverage probability much (i.e. we are operating at very low SINR_R which is where the coverage probability plateaus to 1). Fig. 5.8 shows the naiveté of simply splitting the bandwidth in half. A nearly 2x improvement in transmission capacity is achieved by going from 50% to the optimal allocation of 90%. What is somewhat more surprising is that a 1/25 split (i.e. splitting according to the rate requirement) results in nearly the same performance as a naive 50/50 allocation. Lastly, Fig. 5.8 shows that this allocation is invariant to outage constraint.

Fig 5.9 shows the performance gains in terms of area spectral efficiency that can be achieved by various bandwidth allocations. In all curves, the sum rate of the system is 208Mbps. As expected from Fig. 5.8, the area spectral efficiency is the worst in the naive 50/50 bandwidth allocation. The rate based (96%/4%) allocation performs better, but additional gains can be made by further optimizing the allocation. With the optimal allocation, the two-way system can achieve 75% the area spectral efficiency of the one-way system.

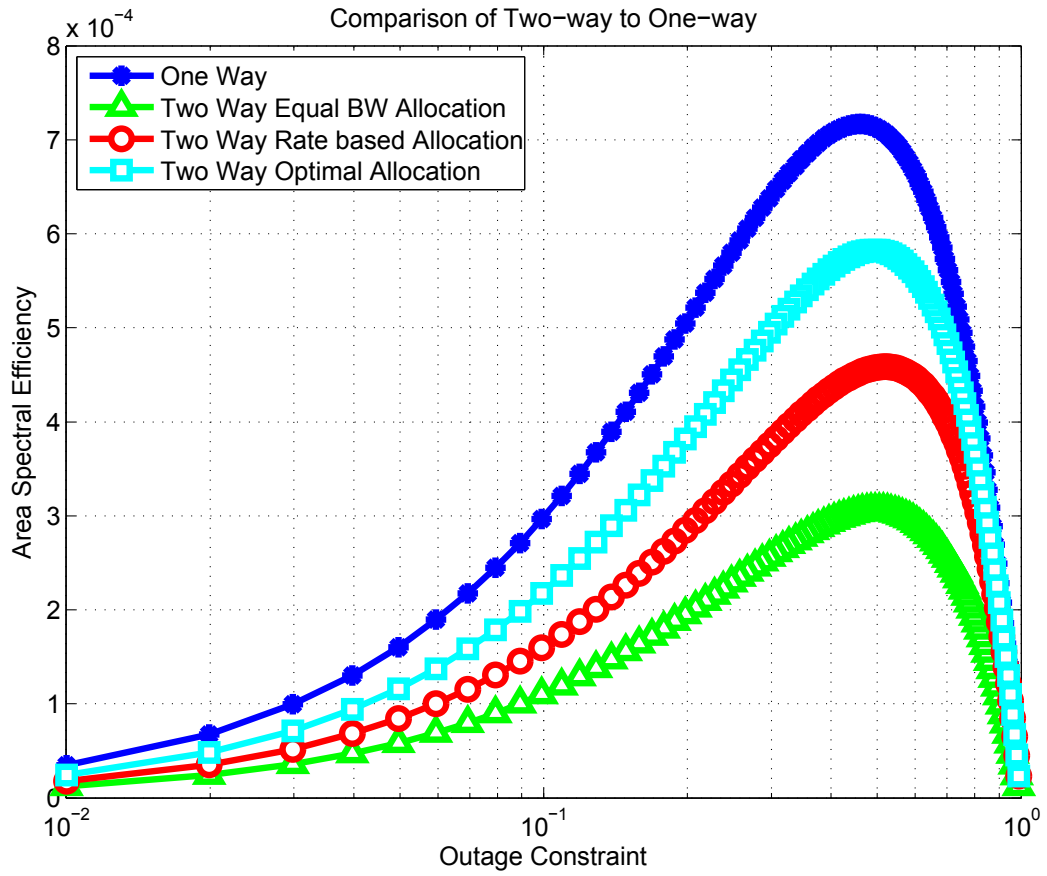


Figure 5.9: Significant gains can be achieved by intelligently allocating bandwidth.

Chapter 6

Conclusion

We presented an analysis that characterized the performance of mmWave ad hoc networks for both one-way and two-way communication. We analyzed the coverage probability, showing that mmWave ad hoc networks have quite favorable SINR distributions even in fairly dense networks. We proposed several reasonable simplifications in order to derive outage-optimal network densities, area spectral efficiency, and the rate coverage of mmWave ad hoc networks. As the next-generation of wireless networks are developed, there are many candidate technologies. We believe that mmWave ad hoc networks can help meet the anticipated $1000\times$ increase in capacity that will be needed for D2D or emergency applications in the coming decade.

Bibliography

- [1] S. Akoum, O. El Ayach, and R.W. Heath. Coverage and capacity in mmwave cellular systems. In *Signals, Systems and Computers (ASILOMAR), 2012 Conference Record of the Forty Sixth Asilomar Conference on*, pages 688–692, 2012.
- [2] A. Alkhateeb, O. El Ayach, G. Leus, and R.W. Heath. Hybrid precoding for millimeter wave cellular systems with partial channel knowledge. In *Information Theory and Applications Workshop (ITA), 2013*, pages 1–5, 2013.
- [3] François Baccelli and Bartłomiej Błaszczyszyn. *Stochastic Geometry and Wireless Networks, Volume II - Applications*, volume 2. NoW Publishers, 2009.
- [4] T. Bai, V. Desai, and R. W. Heath Jr. Millimeter wave cellular channel models for system evaluation. *Proc. of Int. Conf. on Computing, Networking and Commun. (ICNC)*, Feb. 2014.
- [5] T. Bai and R. W. Heath Jr. Coverage analysis for millimeter wave cellular networks with blockage effects. *Proc. of IEEE Global Conf. on Signal and Information Processing (GlobalSIP)*, Dec. 2013.

- [6] T. Bai and R. W. Heath Jr. Coverage in dense millimeter wave cellular networks. In *Signals, Systems and Computers (ASILOMAR), 2013 Conference Record of the Forty Seventh Asilomar Conference on*, 2013.
- [7] T. Bai and R. W. Heath Jr. Coverage and rate analysis for millimeter wave cellular networks. *submitted to IEEE Trans. Wireless Commun.*, March 2014.
- [8] T. Bai, R. Vaze, and R. W. Heath Jr. Analysis of blockage effects on urban cellular networks. *Submitted to IEEE Trans. Wireless Commun.*, Aug. 2013.
- [9] Tianyang Bai, R. Vaze, and R. W. Heath Jr. Using random shape theory to model blockage in random cellular networks. In *Proc. of Int. Conf. on Signal Processing and Communications (SPCOM)*, pages 1–5, Jul. 2012.
- [10] H. Balakrishnan and V. Padmanabhan. Tcp performance implications of network asymmetry.
- [11] Geoffrey Grimmett. *Percolation*.
- [12] Kaibin Huang, J.G. Andrews, Dongning Guo, R.W. Heath, and R.A. Berry. Spatial interference cancellation for multiantenna mobile ad hoc networks. *IEEE Trans. Inf. Theory*, 58(3):1660–1676, 2012.
- [13] A.M. Hunter, J.G. Andrews, and S. Weber. Transmission capacity of ad hoc networks with spatial diversity. *IEEE Trans. Wireless Commun.*, 7(12):5058–5071, 2008.

- [14] T.S. Rappaport, E. Ben-Dor, J.N. Murdock, and Yijun Qiao. 38 ghz and 60 ghz angle-dependent propagation for cellular and peer-to-peer wireless communications. In *Communications (ICC), 2012 IEEE International Conference on*, pages 4568–4573, 2012.
- [15] T.S. Rappaport, Shu Sun, R. Mayzus, Hang Zhao, Y. Azar, K. Wang, G.N. Wong, J.K. Schulz, M. Samimi, and F. Gutierrez. Millimeter wave mobile communications for 5g cellular: It will work! *IEEE Access*, 1:335–349, 2013.
- [16] S. Singh, F. Ziliotto, U. Madhow, E. Belding, and M. Rodwell. Blockage and directivity in 60 ghz wireless personal area networks: from cross-layer model to multihop mac design. *IEEE J. Sel. Areas Commun.*, 27(8):1400–1413, 2009.
- [17] R. Vaze and R.W. Heath. Transmission capacity of ad-hoc networks with multiple antennas using transmit stream adaptation and interference cancellation. *IEEE Trans. Inf. Theory*, 58(2):780–792, 2012.
- [18] R. Vaze, K.T. Truong, S. Weber, and R.W. Heath. Two-way transmission capacity of wireless ad-hoc networks. *IEEE Trans. Wireless Commun.*, 10(6):1966–1975, 2011.
- [19] S. Weber, J.G. Andrews, and N. Jindal. An overview of the transmission capacity of wireless networks. *IEEE Trans. Commun.*, 58(12):3593–3604, 2010.

- [20] Xiaoyi Zhu, A. Doufexi, and T. Kocak. Throughput and coverage performance for IEEE 802.11ad millimeter-wave WPANs. In *Vehicular Technology Conference (VTC Spring), 2011 IEEE 73rd*, pages 1–5, 2011.

Vita

Andrew Scott Thornburg is a graduate student at The University of Texas at Austin. He completed his Bachelors of Science in Electrical and Computer Engineering at the University of Pittsburgh in 2010. He worked as an Electronic Warfare Engineer at Edwards Air Force Base from 2010 – 2012. His research interests span much of wireless communications with a current focus in future mmWave networks.

Permanent address: andrew.thornburg@gmail.com

This report was typeset with \LaTeX^\dagger by the author.

[†] \LaTeX is a document preparation system developed by Leslie Lamport as a special version of Donald Knuth's \TeX Program.